2014

Development of plasmonics-based photoacoustic immunoassay and a photonic crystal substrate for sensitivity enhancement

Yunfei Zhao
Iowa State University

Development of plasmonics-based photoacoustic immunoassay and a photonic crystal substrate for sensitivity enhancement

by

Yunfei Zhao

A thesis submitted to the graduate faculty

in partial fulfillment of the requirements for the degree of

MASTER OF SCIENCE

Major: Electrical Engineering

Program of Study Committee:

Meng Lu, Major Professor

Jaeyoun Kim

Timothy Bigelow

Iowa State University

Ames, Iowa

2014

TABLE OF CONTENTS

LIST OF FIGURES

NOMENCLATURE

ELISA	Enzyme-linked Immunosorbent Assay
PA	Photoacoustic
AuNP	Gold Nanoparticle
IL-8	Interleukin-8
PC	Photonic Crystal
GMR	Guided-mode Resonance
LSPR	Localized Surface Plasmon Resonance
FDTD	Finite Difference Time Domain
AC	Alternating Current
DC	Direct Current
LOD	Limit of Detection
AuNR	Gold Nanorod
HRP	Horseradish Peroxidase
TMB	Tetramethylbenzidine
UV	Ultra-Violet
UVCP	Ultra-Violet Curable Polymer

ACKNOWLEDGEMENTS

I would like to thank my committee chair, Prof. Meng Lu, and my committee members, Prof. Jaeyoun Kim, and Prof. Timothy Bigelow, for their guidance and support throughout the course of this research.

In addition, I would also like to thank my friends, colleagues, the department faculty and staff for making my first two years at Iowa State University a wonderful experience. I want to also offer my appreciation to Prof. John McClelland at Ames Lab, Dr. Wai Leung at Microelectronics Research Center, Mr. Kaiyang Liu and Mr. Yin Huang for their help on my research, without whom, this thesis would not have been possible.

Finally, thanks to my family for their encouragement and to my parents for their hours of patience, respect and love.

ABSTRACT

Immunosandwich assay is an ideal tool for targeted, high-throughput, and quantitative protein analysis. In such an assay, a pair of specific antibodies recognize the analyte, such as a disease biomarker, and the analyte concentration is measured using labels. Conventional immunoassays utilize fluorescent or chemiluminescent dye molecules or enzymes, i.e. enzyme-linked immunosorbent assay (ELISA), as the label to quantify the analyte concentration. By and large, fluorescence-based immunoassays are highly sensitive, but require expensive instrumentations, which limit its application in a point-of-care system in resource-limited settings. In addition, the fluorescent dyes are prone to photobleaching and affected by environmental conditions, which makes the quantitative analysis especially difficult. ELISA uses an inexpensive colorimetric detection system but it lacks the sensitivity to detect low-abundance biomarkers present at the early stage of diseases. To overcome these problems, we proposed a novel photoacoustic (PA) immunoassay using plasmonic nanoparticles to facilitate the detection of disease biomarkers. The principle of PA detection is based on the photothermal effect, in which the absorption of light by target substances generates heat. Illuminated by modulated light from a laser source, the samples will periodically generate heat, which causes the thermal expansion and contraction of the air in the vicinity. The expansion and contraction process results in a pressure wave, which is measured by a microphone. The advantages of the PA detection include a high sensitivity, a large dynamic range, and a low-cost instrumentation. The developed photoacoustic immunoassay uses gold nanoparticles (AuNPs) as a label that converts photons into acoustic waves and reports the analyte concentration. When the laser wavelength matches the

absorbing center of the localized surface plasmon resonance, the collective oscillation of free electrons within AuNPs results in a significantly stronger photoacoustic conversion. The intensity of the acoustic wave generated by the AuNPs is correlated to the analyte concentration. The plasmonic-enhanced PA effect offers a highly sensitive and reliable approach for the detection of biomarkers. As an example, the PA assay of Human interleukin-8 (IL-8) was carried out using our PA detector and the results show a limit of detection of 1.6 pg/mL, which is one order of magnitude lower than the standard colorimetric assay.

To further improve the detection sensitivity, a nanostructured substrate was implemented to enhance the light absorption of the AuNPs. The substrate consists of a photonic crystal (PC) structure, which supports the guided-mode resonance (GMR), also known as the leaky mode resonance. When a laser light is coupled into a GMR mode, the resulting evanescent field near the PC surface is significantly enhanced compared to the intensity of the excitation beam. The enhanced near field allows the AuNPs, immobilized in the evanescent field region, to absorb more light and to consequently generate a stronger PA signal. It has been demonstrated that the PC substrate can improve the PA signal by a factor of 40 and enable the measurement of less than 10 AuNPs in an area of 100 μm^2.

CHAPTER 1

INTRODUCTION

1.1 Research Objective

The objective of this research is to develop a plasmonics-based PA immunoassay and to increase the sensitivity of detecting trace amounts of biomarkers by an order of magnitude compared to currently used immunoassay techniques. This work also focuses on the further enhancement of the PA signal by using a PC substrate. This is very important because the PC substrate can potentially enable single-particle level sensitivity of the detection of AuNPs.

1.2 Research Motivation

The ability to detect trace amounts of biomarkers related to certain diseases is long sought for in modern diagnostics. The current techniques utilize fluorescent or chemiluminescent dye molecules or enzymes, for example, ELISA, as the label to quantify the analyte concentration. By and large, fluorescence-based immunoassays are highly sensitive, but require expensive instrumentations, which limit its application in a point-of-care system in resource-limited settings. In addition, the fluorescent dyes are prone to photobleaching and affected by environmental conditions, which makes the quantitative analysis especially difficult. ELISA uses an inexpensive colorimetric detection system but it lacks the sensitivity to detect low-abundance biomarkers present at the early stage of diseases.

Owing to the strong interaction between the incident optical field and the localized surface plasmon resonance (LSPR) of metal nanoparticles, the PA effect can be used to effectively detect small amounts of metal nanoparticles. By utilizing metal nanoparticles as tags

to detect target biomarkers, one can significantly increase the sensitivity of detecting certain biomarkers by using a PA based detection method. Apart from high sensitivity, PA detection has other advantages such as a large dynamic range, low cost instrumentations and stabler samples, which are not susceptible to photobleaching and can be stored for a long duration. Therefore, the development of a PA immunoassay based on the LSPR of AuNPs can potentially increase the sensitivity of biomarker detection significantly while lowering the cost and hence widen the accessibility of biomarker detection assays, which is very favorable for early diagnosis of certain diseases, especially in resource-limit settings.

1.3 Organization of the Thesis

Principles of PA effect and LSPR of plasmonic nanoparticles are important for such a PA immunoassay to be developed. Chapter 2 introduces the mechanism of PA effect, the experimental setup for the measurement of PA effect and a quantitative description of the intensity of the PA signal generated by this setup. Also the mechanisms of the LSPR of plasmonic nanoparticles and the enhancement of optical absorption are briefly introduced.

Chapter 3 reports the characterization of PA signal. The dependence of the intensity of PA signals on the modulation frequency, the input power of incident light and the concentration of AuNPs is studied. This helps the choice of experiment apparatus and parameters in the subsequent experiments.

Chapter 4 discusses the development of plasmonics-based PA immunoassay. Details regarding the steps of conventional ELISA experiment and PA immunoassay are reported. The relationship between optical absorbance and target biomarker concentration in the sample as well as that between PA signal and target biomarker concentration are obtained.

Chapter 5 discusses the further enhancement of PA signal by using a PC substrate. The fabrication of the PC substrate as well as the enhancement mechanism, the GMR mode, are treated in detail. Finite difference time domain (FDTD) simulations of the near field enhancement of the PC substrate and the PA detection of an absorbing dye very low concentrations of AuNPs are carried out and the enhancement by PC substrate is verified.

Chapter 6 draws some conclusions about the research. The future work for this research as well as some practical applications of the PA immunoassay and PA detection are suggested.

CHAPTER 2

PHOTOACOUSTIC EFFECT AND LOCALIZED SURFACE PLASMON RESONANCE

2.1 Principle of Photoacoustic Effect

Photoacoustic effect is the formation of sound waves following light absorption by a material sample. It is caused by photothermal effect in which materials absorb optical energy and eventually convert it into thermal energy [1]. The origin of photothermal effect is the process in which photons of the incident light excite electrons in absorbing materials from the ground state to excited states, and then the excited electrons lose their energy by a series of non-radiative transitions, resulting in heating of the materials [1]. Usually, such heating is very weak. Therefore, the best way to measure such weak heating is by modulating it, so that it appears in the form of an AC component and can be processed independently of the larger DC component. By periodically modulating the incident light on the absorbing materials, the heat will be generated periodically as well, producing a periodic temperature change. This change then causes the air in the vicinity of the sample to undergo periodic thermal expansion and contraction, producing a pressure wave, which is converted by a microphone into an AC electrical signal and is processed or amplified using various instruments such as a pre-amplifier or a lock-in amplifier. The amplified signal is then displayed with an oscilloscope.

The schematic diagram of a photoacoustic detection system is shown in Figure 1, in which the incident light generated by a certain light source (Xenon lamp, laser, etc.) is modulated by a mechanical chopper and illuminated upon the sample placed inside an air-tight PA cell, which prevents outer noise from coming into the microphone and pressure waves generated by

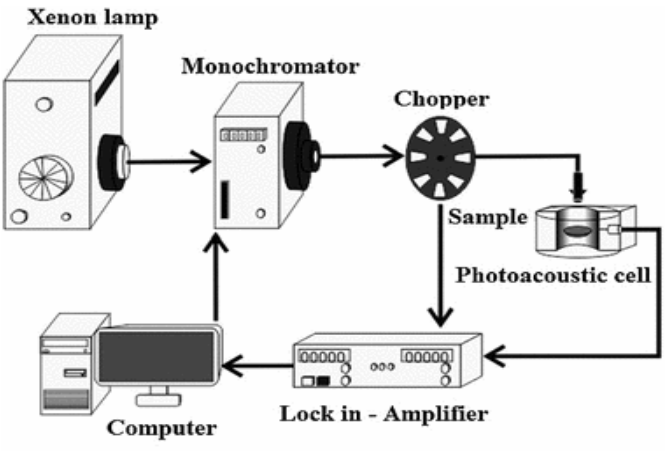

Figure 1. Schematic diagram of a PA detection system [2]

the sample from propagating out of the cell. Then the pressure waves are detected by a microphone also placed inside the cell and an AC electrical signal is generated, amplified and displayed. The peak pressure change in the pressure wave can be calculated as [3]:

$$\delta P \propto \frac{\alpha \beta E_L}{C_p \tau^{3/2}} \sqrt{\frac{c}{r}} \tag{1}$$

where α is the optical absorption coefficient, β is the volume expansion coefficient of the air, E_L is the excitation energy per cycle of the modulated light, C_p is the specific heat capacity, c is the speed of sound in air, r is the radial distance between the transducer and the source and τ is the pressure perturbation time, which is the root mean square of the relaxation times and the pulse or modulation width.

2.2 Localized Surface Plasmon Resonance

According to Eq. (1), a material with strong optical absorption (high α) is needed to facilitate the detection of trace amount of biomarkers with photoacoustic method. AuNP is an

ideal light-absorbing material that has a very high optical absorbance due to its LSPR. Therefore, using AuNPs as tags to label biomolecules can significantly boost the sensitivity and limit of detection (LOD). LSPR is a phenomenon in which the free electrons in a metal nanoparticle coherently oscillate in response to the optical field of the incident light [4]. It happens when the size of the metal nanoparticles is smaller than the wavelength of the incident light, as shown in Figure 2. The near field intensity of the AuNPs is enhanced when the resonance conditions are satisfied, resulting in an enhanced absorption of the incident light [5]. The near field distribution of a dipole LSPR mode when a gold nanosphere is illuminated by an electromagnetic plane wave $\boldsymbol{E_0} = E_0\hat{\boldsymbol{z}}$ can be expressed as [6]:

$$\boldsymbol{E}_{\boldsymbol{out}}(x,y,z) = E_0\hat{\boldsymbol{z}} - \alpha E_0\left[\frac{\hat{\boldsymbol{z}}}{r^3} - \frac{3z}{r^3}(x\hat{\boldsymbol{x}} + y\hat{\boldsymbol{y}} + z\hat{\boldsymbol{z}})\right] \tag{2}$$

where α is the metal dipole polarizability and can be further expressed as:

$$\alpha = ga^3 \tag{3}$$

where a denotes the diameter of the nanosphere and g denotes the dipole magnification factor, which is defined as:

$$g = (\varepsilon_m - \varepsilon_b)/(\varepsilon_m + 2\varepsilon_b) \tag{4}$$

in which $\varepsilon_m = \varepsilon_{mr} + i\varepsilon_{mi}$ is the complex dielectric function of the metal and ε_b is the dielectric constant of the surrounding medium. To get a maximum near field enhancement, the dipole magnification factor g needs to be maximized, therefore the denominator of g needs to be minimized. This is fulfilled when the resonance condition, $\varepsilon_{mr} + 2\varepsilon_b = 0$, is satisfied. The absolute square of $\boldsymbol{E}_{\boldsymbol{out}}$ is given by:

$$E_{out}^2 = E_0^2|g|^2(1 + 3cos^2\theta) \tag{5}$$

From Eq. (5) we can see that the absolute square of $\boldsymbol{E}_{\boldsymbol{out}}$ is proportional to the absolute square of

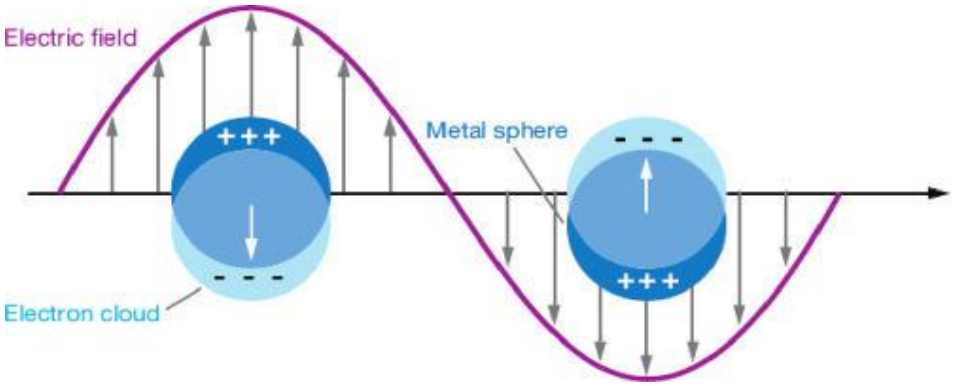

Figure 2. Localized surface plasmon resonance of metal nanoparticles [7]

the dipole magnification factor. In this work, biomolecule-conjugated gold nanorods (AuNRs) were used to tag target biomarkers since they have a stronger LSPR than traditional spheroidal AuNPs [8, 9].

CHAPTER 3

PRELIMINARY CHARACTERIZATION OF PA EFFECT

Before the measurement of AuNP tagged biomarkers, some preliminary studies regarding the relationships between the intensity of the PA signal and the intensity of the incident light, the modulation frequency and the AuNP concentration needs to be studied. In this study, AuNRs with a length of 60 nm and an axial diameter of 25 nm were used. The aspect ratio of the AuNRs was 2.4. From the simulation results shown in Figure 3, the absorption peak will be at approximately 600 nm. The laser used was a He-Ne laser with an output of 5.86 mW

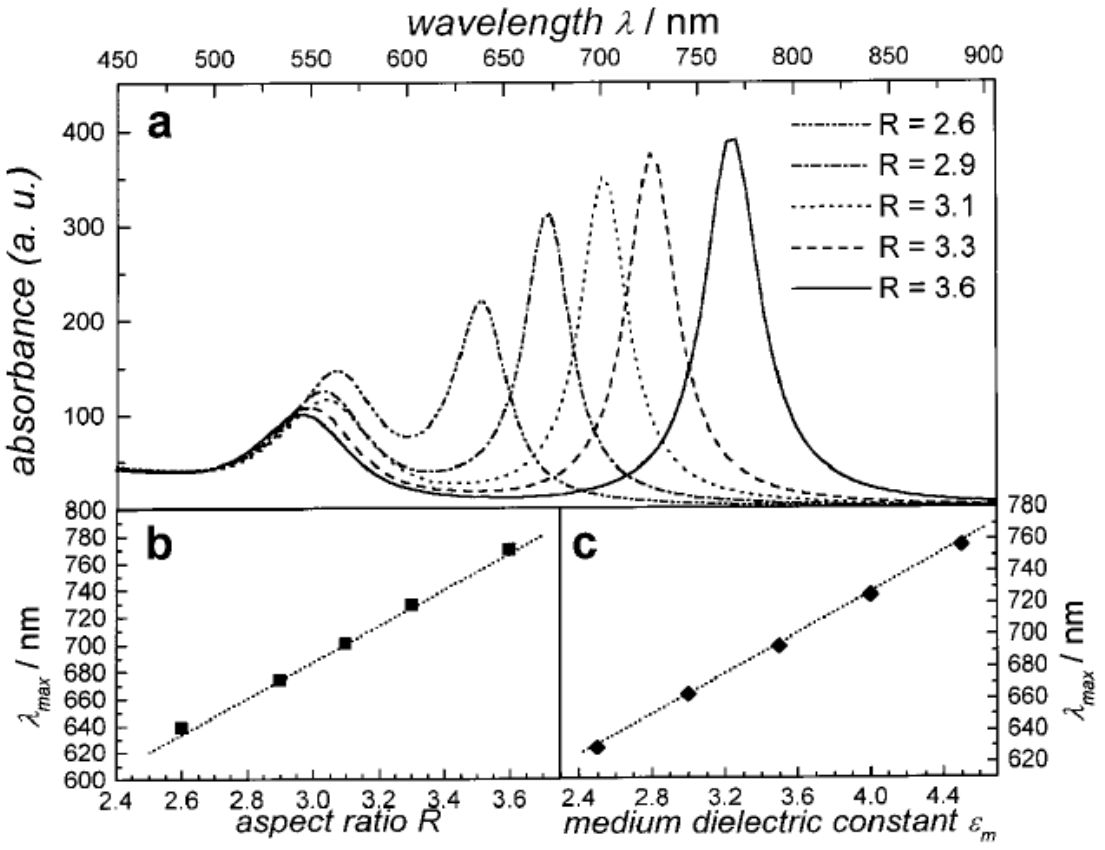

Figure 3. Simulation of absorption peaks of AuNRs with respect to aspect ratio [8]

at a wavelength of 632.8 nm, which was in the full width at half maximum of the absorption peak. The AuNRs were in the form of water suspension with a concentration of 10^{12} NPs/mL. The sample was made by dipping 10 μL of AuNR suspension onto a circular acrylic window of a low thermal mass with a diameter of 18 mm and letting the water dry. The AuNRs covered an area of approximately 100 mm^2. The PA unit used was a PAC 200 (MTEC Photoacoustis Inc.) PA unit, and the PA signal was displayed with an oscilloscope (TDS 2000, Tektronix). The first measurement was the relationship between the PA signal and the modulation frequency. The output of the laser beam was kept at 5 mW and the frequency was changed by changing the rpm of the chopper. The PA signals at frequencies of 13 Hz, 26 Hz, 52 Hz, 104 Hz, 208 Hz, 416 Hz, 832 Hz and 1185 Hz were measured. As shown in Figure 4, the PA signal was inversely proportional to the chopping frequency. This can be largely explained by the proportionality of

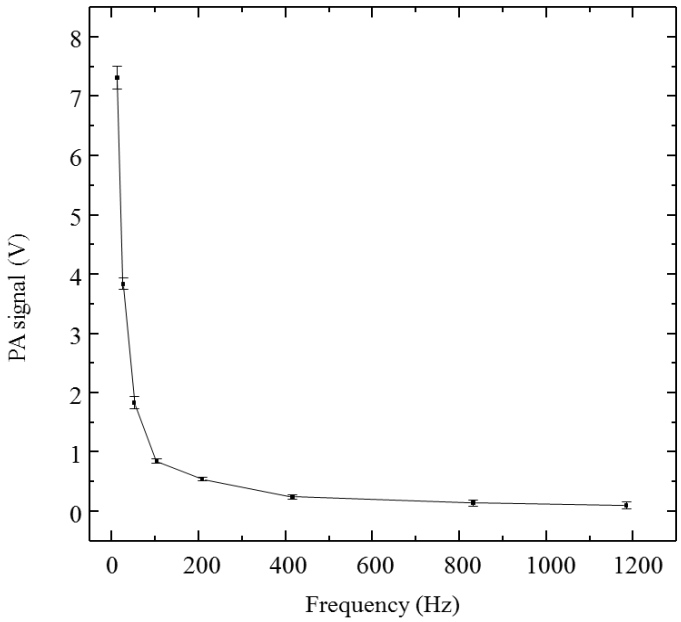

Figure 4. PA signal with respect to chopping frequency

the PA signal with respect to the excitation energy per cycle E_L, which is in turn proportional to the duration of heating and cooling in each cycle. The chopper modulated the incident laser in a square wave pattern, with a duty cycle of 50%. As a result, the temperature of the sample would increase linearly in the heating cycle and decrease linearly in the cooling cycle, forming a triangular waveform. As the sample was placed in an air-tight chamber, the pressure of the air in the chamber would also increase and decrease linearly with the temperature, as indicated by the ideal gas law, resulting in a triangular waveform PA signal. The amplitude of the PA signal was therefore proportional to the amplitude of the temperature oscillation, which was proportional to the heating and cooling cycle, and hence the chopping period, or in other words, inversely proportional to the chopping frequency. The relationship between the PA signal and the intensity of the incident light was also examined using the same sample and equipment. The frequency was kept at 13 Hz and the intensity of the incident light was serially reduced using a neutral

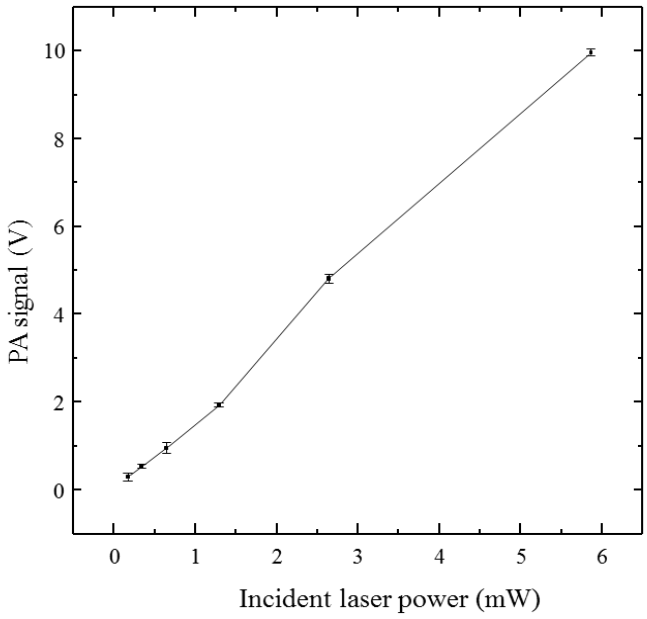

Figure 5. PA signal with respect to incident laser power

density filter. The PA signals at the output power of 5.86 mW, 2.64 mW, 1.29 mW, 0.645 mW, 0.34 mW and 0.17 mW were measured. As shown in Figure 5, the PA signal decreased largely linearly with decreasing incident laser power, which can also be explained by the proportionality of the PA signal with respect to the excitation energy per cycle E_L.

The relationship between the PA signal and the concentration of AuNPs, which is crucial to the quantification of biomarkers, was subsequently studied. In this experiment, the chopping frequency was kept at 13 Hz and the incident laser power was kept at 5.86 mW. The PA signals of samples with AuNP concentrations of 10^{12} NPs/mL, 10^{11} NPs/mL, 10^{10} NPs/mL and 10^{9} NPs/mL were measured and plotted in Figure 6. The signal was largely linear with respect to the concentration of AuNP (the curve is not straight because the horizontal axis is in logarithm scale), which was favorable for the quantification of biomarker concentration.

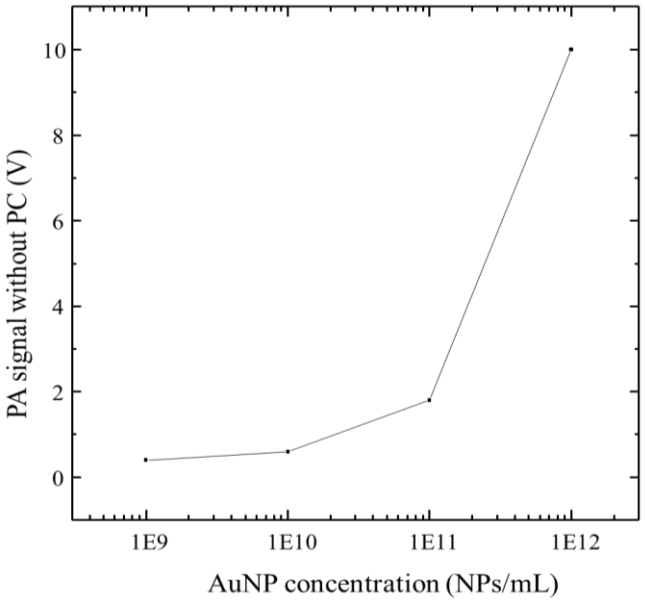

Figure 6. PA signal with respect to AuNP concentration

CHAPTER 4

PLASMONICS-BASED PHOTOACOUSTIC IMMUNOASSAY AND ITS APPLICATION IN THE DETECTION OF HUMAN IL-8

Human IL-8 is a chemokine produced mainly by macrophages, as well as other cells such as airway smooth muscle cells, endothelial cells and epithelial cells [10]. It is related to various inflammation and diseases such as gingivitis [11], psoriasis [12], obesity [13], and schizophrenia [14, 15]. The ELISA kit for human IL-8 is one of the most common, lowest-cost and most accessible ELISA kits for research purposes, thus we chose to develop a PA immunoassay to quantify human IL-8 as a demonstration to test the feasibility of the PA method. A conventional ELISA experiment using a colorimetric quantification method based on the direct measurement of the absorbance of the samples was carried out first for reference purposes. The steps of such a conventional ELISA experiment are as follows: first, 50 μL of serially diluted human IL-8 standards were added to each well in duplicate. The plate was then covered and incubated at room temperature for 1 hour. The bottoms of the wells were precoated with anti-human IL-8 antibody that acted as the capture antibody to immobilize human IL-8 onto the surface. Then the plate was washed three times to get rid of unbound human IL-8 and 50 μL of biotinylated antibody reagent was added to each well subsequently. The biotinylated antibody acted as the detection antibody to bind with human IL-8. After 1 hour of incubation at room temperature, unbound biotinylated antibody was washed away and 100 μL of streptavidin-horseradish peroxidase (HRP) solution was added to each well. The streptavidin-HRP would bind with the biotinylated antibody via biotin-streptavidin binding and the HRP would act as the enzyme to catalyze a colorimetric reaction in the following step. After incubation at room temperature for

30 minutes, the plate was washed for three times again to remove unbound streptavidin-HRP. After washing the plate, 100 µL of tetramethylbenzidine (TMB) substrate solution was added to each well and the plate was developed at room temperature in the dark for 30 minutes. The TMB would undergo a colorimetric reaction due to the catalysis of HRP. The concentration of HRP bound to the detection antibody was different in each well, due to the difference in human IL-8 concentration, which would result in a difference in the reaction rate of the colorimetric reaction. After 30 minutes of development, 100 µL of TMB stop solution was added to each well to stop the colorimetric reaction. Therefore, the difference of the reaction rate would result in a difference in the concentration of reaction product, which was in turn reflected by the difference in the color of the reaction product. The optical absorbance of the reaction product in each well was then measured with a plate reader and the difference in absorbance at the wavelengths of 450 and 550 nm were calculated as the final result. The concentrations of the

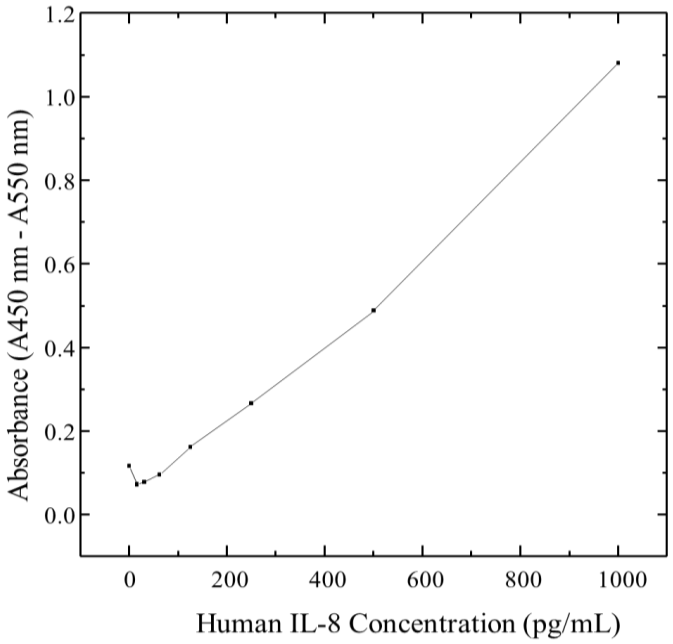

Figure 7. Standard curve for human IL-8 ELISA measured with colorimetric method

serial dilutions of the human IL-8 of the human IL-8 standards were 1000 pg/mL, 500 pg/mL, 250 pg/mL, 125 pg/mL, 62.5 pg/mL, 31.25 pg/mL, 16.06 pg/mL, and 0 pg/mL as a control. The lowest dilution the colorimetric method can detect was 16.06 pg/mL, as indicated by the absorbance with respect to standard concentration curve in Figure 7. From Figure 7 we note that the direct measurement of optical absorbance did not yield an accurate result at very low concentrations, as the result for the control deviated from the linearly decreasing trend of the curve.

The PA immunoassay was developed based on the existing ELISA format, with the only difference being the substitution of streptavidin-conjugated AuNR suspension for the streptavidin-HRP solution and the removal of the subsequent steps relating to the streptavidin-HRP solution. Therefore to be specific, the steps from the substitution of streptavidin-HRP are

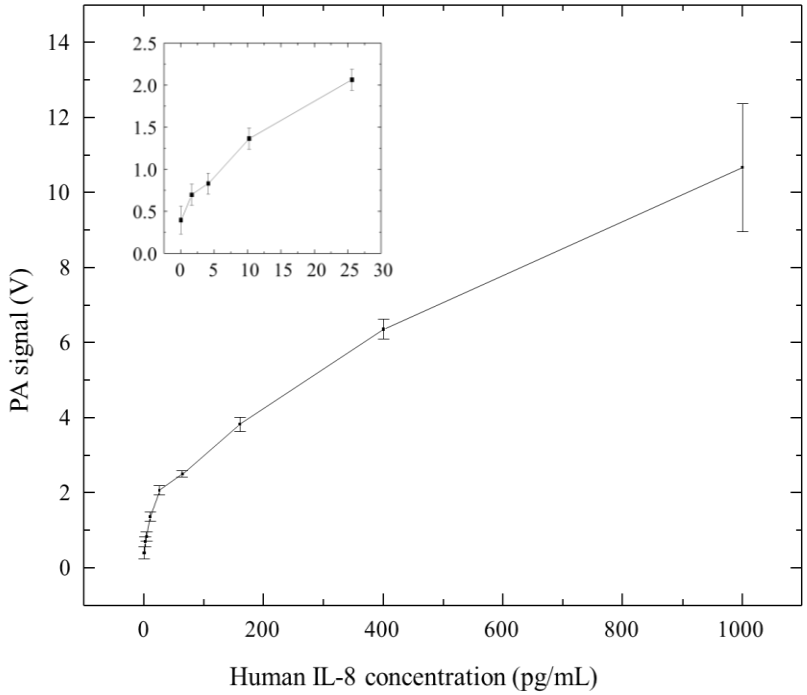

Figure 8. PA signal with respect to human IL-8 concentration

as follows: instead of adding 100 μL of streptavidin-HRP to each well, 100 μL of streptavidin-conjugated AuNR suspension with a concentration of 10^{12} NPs/mL (nanoparticles per mL) was added to each well. Then the plate was incubated for 30 minutes at room temperature and washed three times to remove unbound AuNRs subsequently. After washing and drying the plate naturally in air, the PA signal of each well was measured with aforementioned apparatus and plotted against the concentration of AuNRs bound to the bottom of each well in Figure 8. The serially diluted standards used in the PA immunoassay had concentrations of 1000 pg/mL, 400 pg/mL, 160 pg/mL, 64 pg/mL, 25.6 pg/mL, 10.2 pg/mL, 4.1 pg/ml, 1.6 pg/mL and 0 pg/mL as a control. The PA signal was largely linear at low concentration levels, while at higher concentration levels, due to steric hindrance of AuNRs the PA signal deviated from linear increase with the concentration of human IL-8. It is worth noting that the current result of PA detection shows that the LOD was 1.6 pg/mL, an order of magnitude lower than that of the colorimetric detection method based on direct measurement of optical absorbance. This is due to absorption enhancement by the LSPR of the AuNRs.

In conclusion, the PA immunoassay is capable of improving the LOD of conventional ELISA by an order of magnitude. By optimizing the experiment protocols for the PA immunoassay, we believe that it has a potential of further decreasing the LOD to below 1 pg/mL.

CHAPTER 5

FURTHER ENHANCEMENT OF PA SIGNAL BY USING A PHOTONIC CRYSTAL SUBSTRATE

As we can see in the results of the PA immunoassay, at low concentrations the main obstacle of further increasing the sensitivity is the noise, as indicated by the error bars. Therefore the bottleneck of the PA immunoassay is the signal-to-noise ratio when the analyte concentration is very low. To address this issue and to attain a higher accuracy of quantifying trace amounts of target molecules, we propose the use of a 1-D photonic crystal (PC) substrate to enhance the optical absorption of AuNPs and hence the PA signal. The PC substrate supports guided-mode resonance (GMR), also known as a leaky mode [16-18]. When the PC substrate is illuminated under resonance conditions (by an incident light of certain wavelength at a certain incident angle), the near field intensity on the surface of the PC substrate will be greatly enhanced compared to the optical field intensity of the incident light. By spectrally overlapping the resonance wavelength with the absorption band of the analyte residing on the PC substrate, one can significantly boost the optical absorption, and hence the PA signal of the analyte. Shown in Figure 9 is a cross-sectional diagram of the 1-D PC substrate (not to scale). It was fabricated with a nanoreplica molding process [19]. Briefly, a 2 mm × 2 mm silicon mold bearing a grating pattern was first fabricated using electron beam lithography and reactive ion etching. Then, ultra-violet curable polymer (UVCP) was squeezed between the silicon mold and a transparent acrylic film and solidified by UV exposure. After separation from the mold, the substrate film with the UVCP carried a grating pattern with a period of 400 nm, a depth of 60 nm

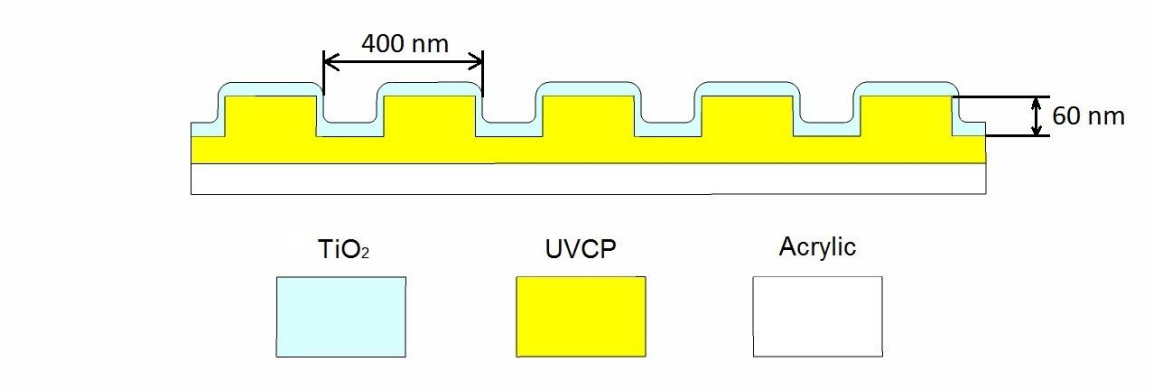

Figure 9. Cross-sectional diagram of the 1-D PC structure [20]

and a duty cycle of 60%. A TiO_2 coating with a thickness of 100 nm was coated via electron beam evaporation onto the UVCP. It has a higher refractive index (n = 2.60) than that of the UVCP (n_{UVCP} = 1.46), which provides light confinement for the GMR. The aforementioned parameters were chosen in order to maximize the strength of the optical resonance at the exciting wavelength and hence to attain maximum near field intensity.

To make sure the resonance conditions are satisfied during the measurement, we designed an optical setup as shown in Figure 10. It consisted of a He-Ne laser at 632.8 nm as a light source, a mechanical chopper, and a PA chamber with a sample and a microphone placed inside, which are standard components of a PA detection system. To satisfy the resonance condition at the wavelength of 632.8 nm, a mirror M1 and a convex lens were added into the optical path. Both of them can be translated along the directions indicated by the arrows. The translation of the convex lens ensured that the focal point lied on the sample, so that the translation of mirror M1 tuned the incident angle of the laser onto the PC substrate without changing the point of incidence. The function of the second mirror M2 is merely to direct the laser to the sample.

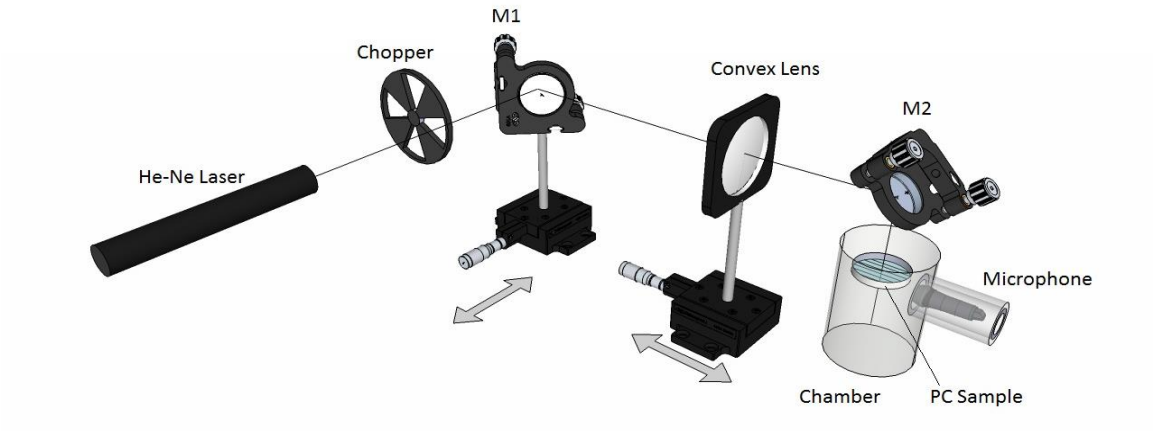

Figure 10. Complete experiment layout of the optical setup for PC enhanced PA detection [20]

After the setup was established, an absorbing dye (Epolight 5262, Epolin Inc.) was used to test the performance. The angle dependence of normalized transmission coefficient and the PA signal of the absorbing dye are plotted in Figure 11. As shown in the figure, there is a dip in

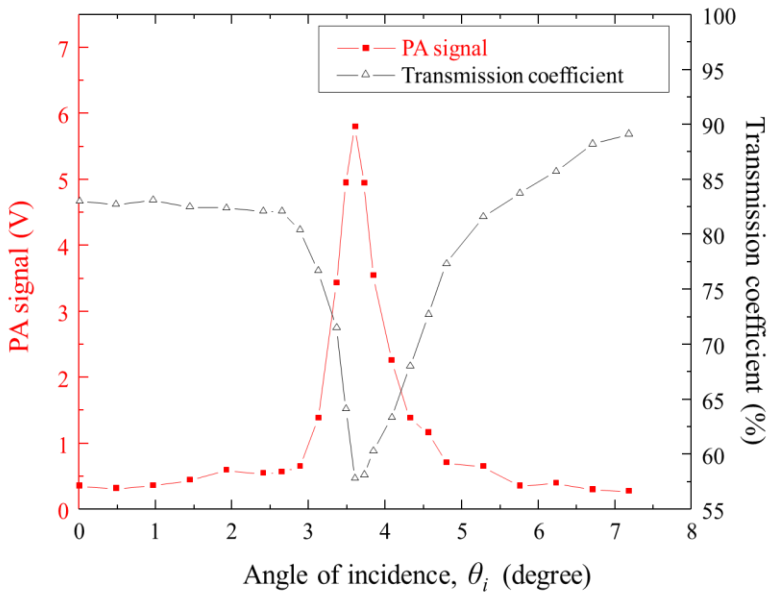

Figure 11. Angle dependence of PA signal and transmission coefficient for absorbing dye on a PC substrate [20]

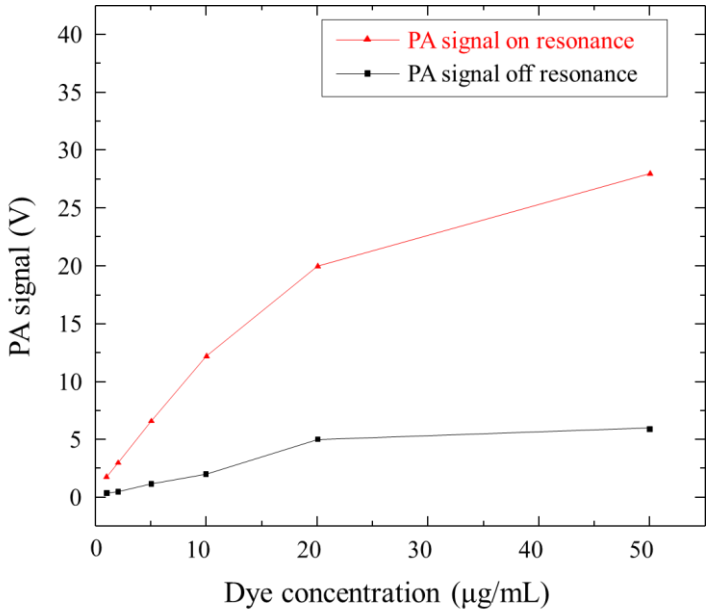

Figure 12. PA signal for a dilution series of absorbing dyes spread on a PC substrate measured on- and off-resonance [20]

the transmission curve at the angle of incidence of 3.5°, indicating that the optical resonance conditions were satisfied. A peak in the PA signal occurred in exact accordance with the dip in transmission. After subtracting the background noise, the PA signal measured under on resonance conditions was 10× higher than that measured under off-resonance conditions, confirming the PA signal enhancement by optical resonance. In addition, a dilution series from 50 μg/mL to 1 μg/mL were measured in both on-resonance and off-resonance conditions. Figure 12 shows a comparison between the PA signals of absorbing dye measured at on-resonance and off-resonance conditions. In the linear range from 0 to 20 μg/mL, the PA signal measured under on-resonance conditions had a sensitivity of 1.25 V/(μg/mL), compared to the 0.18 V/(μg/mL) measured under off-resonance conditions, an increase of 7-fold.

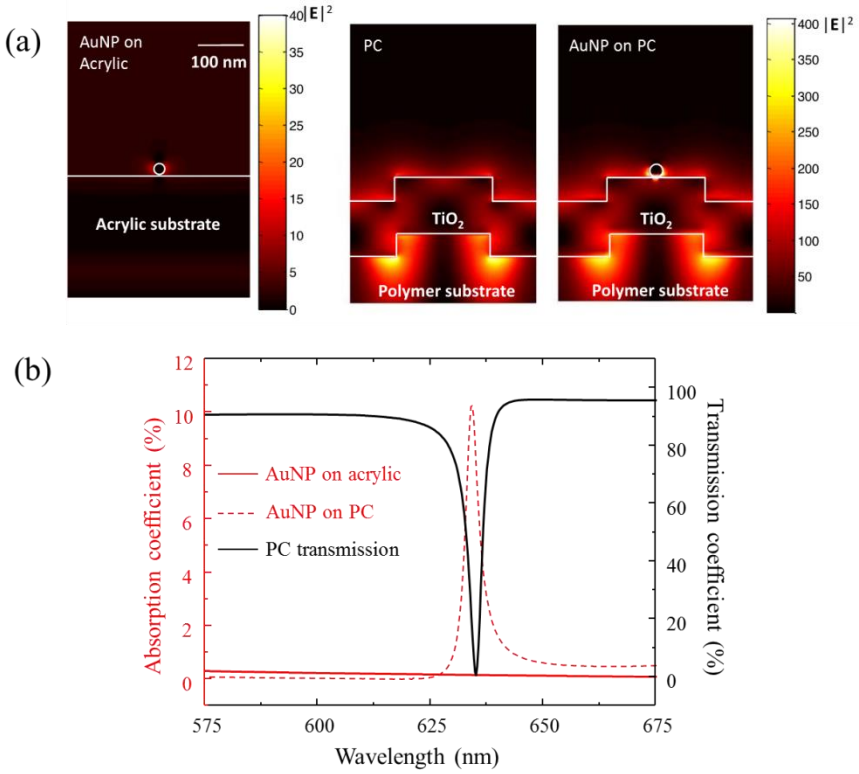

Figure 13. FDTD simulation results for a AuNP on a flat acrylic surface, a PC substrate without a AuNP, and a AuNP on a PC substrate [20]

Having demonstrated the enhancement of PA signal of the absorbing dye by the PC substrate, we next exploited the enhancement of PA signal generated by AuNPs. FDTD simulations were carried out to calculate the near field distribution under following settings: a AuNR residing on a plane acrylic surface; a PC surface without a AuNR; and a AuNR residing on a PC surface. In the simulation, a plane wave at 632 nm was set to incident normally onto the surfaces and the PC structure was realized by applying periodic boundary conditions to the 2nd and 3rd settings. The intensity of the electric field $|E|^2$ normalized with respect to that of the incident optical field was visualized in Figure 13 (a). As shown in the figure, the evanescent field near the surface of the PC substrate as well as that in the vicinity of the AuNP was significantly enhanced. Plotted in Figure 13 (b) is the calculated transmission and optical

absorption of AuNPs with respect to incident wavelength. The enhancement in optical absorption correlated well with the GMR mode, with an enhancement factor of 60×.

The angle dependence of PA signal of AuNPs was measured and the detection of a 10-fold serial dilution of AuNP suspensions from 10^{12} NPs/mL to 10^{9} NPs/mL using the PC substrate was carried out using the aforementioned method and apparatus. The results are shown in Figures 14 and 15. The PA signal on resonance at the angle of incidence 3.2 °was 13 V and 40× stronger than the PA signal off resonance which is 0.33 V. The LOD of the AuNPs was improved by an order of magnitude from 10^{10} NPs/mL to 10^{9} NPs/mL by the application of a PC substrate, as shown in Figure 15. At higher concentrations, the enhancement factor decreased due to quench caused by high concentration levels of AuNPs. The PC substrate allowed the detection of less than 10 AuNRs per 100 μm^2, which was close to single-particle level sensitivity, as indicated by the SEM image of the AuNRs on the PC substrate shown in the inset of Figure 14.

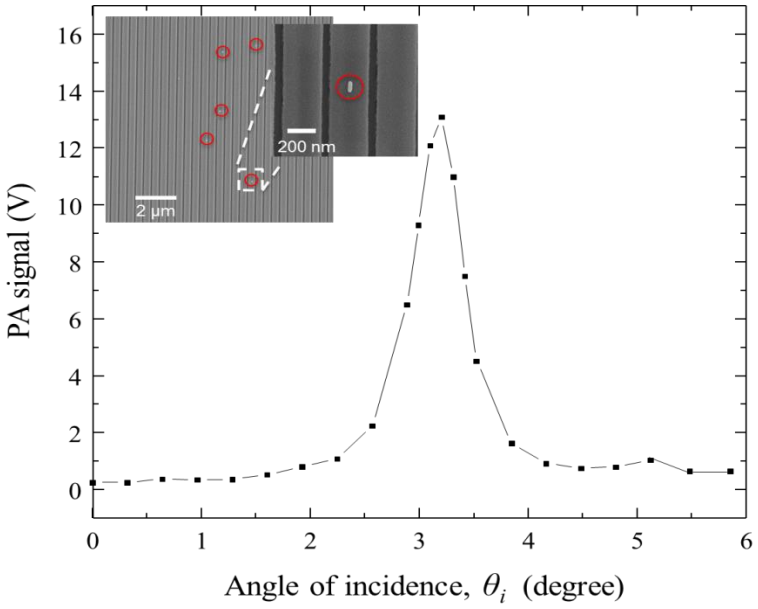

Figure 14. Angle dependence of PA signal of AuNPs on a PC substrate [20]

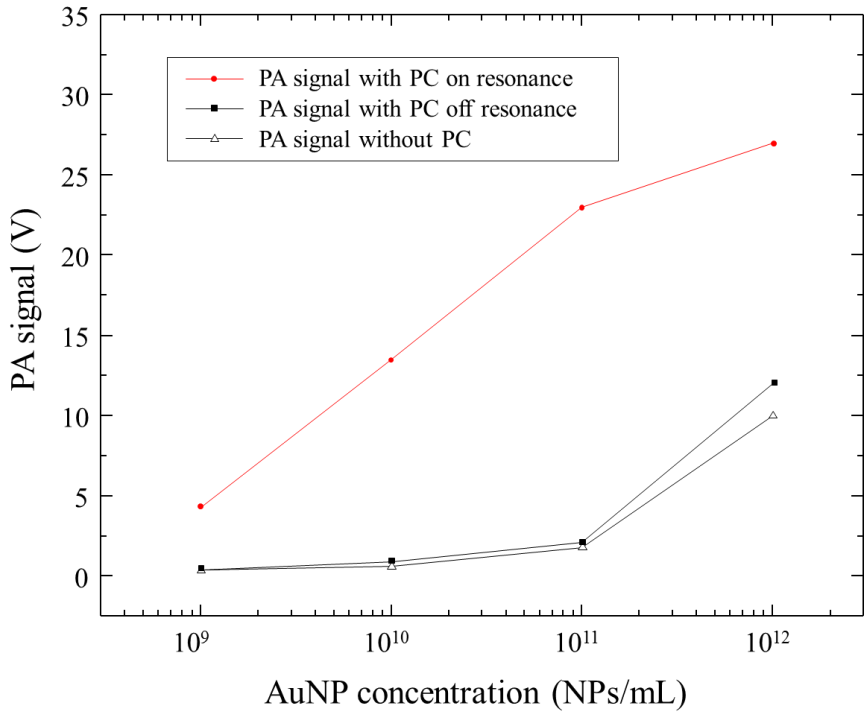

Figure 15. PA signals for a dilution series of gold nanoparticles spread on a PC substrate and an acrylic substrate, respectively [20]

CHAPTER 6

CONCLUSIONS

In summary, a PA immunoassay protocol was developed based on the ELISA format and human IL-8 is quantified using this method as an example. The method used AuNPs as a tag to label biomarkers and used a standard laser-based PA detection system to quantify the concentration of AuNPs. The LOD was increased by an order of magnitude using this method. The PA detection was further enhanced by using a PC substrate. The GMR of the PC substrate significantly enhanced the near field intensity compared to the input optical field intensity and a limit of detection of less than 10 AuNRs per 100 μm^2 was attained. In the future, a hand-held PA unit that can fit into a single well of the microtiter plate will be developed and the sensitivity will be improved even further, enabling a promising approach for point-of-care diagnostic system and environmental monitoring.

REFERENCES

1. D. P. Almond, P. M. Patel, *Photothermal Science and Techniques* (Chapman & Hall, London, 1996).

2. R. Rico Molina, C. Hernandez Aguilar, A. Dominguez Pacheco, A. Cruz-Orea, J. L. Lopez Bonilla, "Characterization of maize grain with different pigmentation investigated by photoacoustic spectroscopy," *International Journal of Thermophysics*, DOI: 10.1007/s10765-013-1445-8, 2013

3. C. Kelly, J. Leis and D. Buttsworth, "Development of a photo-acoustic trace gas sensor," *Proceedings of ACOUSTICS*, pp. 139-146, 2011

4. S. Zeng, K. Yong, I. Roy, X. Dinh, X. Yu, F. Luan, "A review on functionalized gold nanoparticles for biosensing applications," *Plasmonics*, vol. 6, pp. 491-506, 2011

5. S. Wang, S. Boussaad, N. J. Tao, "Surface plasmon resonance enhanced optical absorption spectroscopy for studying molecular adsorbates," *Review of Scientific Instruments*, vol. 72, no. 7, pp. 3055-3060, 2001

6. D. Mortazavi, A. Z. Kouzani1, A. Kaynak, and W. Duan, "Developing LSPR design guidelines," *Progress In Electromagnetics Research*, vol. 126, pp. 203-235, 2012

7. K. A. Willets, R. P. Van Duyne, "Localized surface plasmon resonance spectroscopy and sensing," *Annu.. Rev. Phys. Chem.* vol. 58, pp. 267-97, 2007

8. S. Eustis, M. A. El-sayed, "Determination of the aspect ratio statistical distribution of gold nanorods in solution from a theoretical fit of the observed inhomogeneously broadened longitudinal plasmon resonance absorption spectrum," *J. Appl. Phys.* **100**, 044324, 2006

9. S. Link, M. A. El-Sayed, "Spectral properties and relaxation dynamics of surface plasmon electronic oscillations in gold and silver nanodots and nanorods," *J. Phys. Chem. B*, vol. 103, pp. 8410-8426, 1999

10. J. C. Hedges, C. A. Singer, W. T. Gerthoffer, "Mitogen-activated protein kinases regulate cytokine gene expression in human airway myocytes," *Am. J. Respir. Cell Mol. Biol.*, vol. 23, no. 1, pp. 86–94, 2000

11. S. K. Haake, G. Huang: Molecular Biology of the host-Microbe Interaction in Periodontal Diseases (Selected Topics). In Newman, Takei, Carranza, editors: *Clinical Periodontology*, 9th Edition. Philadelphia: W.B.Saunders Co. p. 162, 2002

12. B. Wolff, A. R. Burns, J. Middleton, A. Rot, “Endothelial cell "memory" of inflammatory stimulation: human venular endothelial cells store interleukin 8 in Weibel-Palade bodies,” *J. Exp. Med.*, vol. 188, no. 9, pp. 1757–62, 1998

13. K. Bacon, M. Baggiolini, H. Broxmeyer, R. Horuk, I. Lindley, A. Mantovani, K. Maysushima, P. Murphy, H. Nomiyama, J. Oppenheim, A. Rot, T. Schall, M. Tsang, R. Thorpe, J. Van Damme, M. Wadhwa, O. Yoshie, A. Zlotnik, K. Zoon, “Chemokine/chemokine receptor nomenclature,” *J. Interferon Cytokine Res.*, vol. 22, no. 10, pp. 1067–8, 2002

14. D. Bhaumik, G. K. Scott, S. Schokrpur, C. K. Patil, A. V. Orjalo, F. Rodier, G. J. Lithgow, and J. Campisi, “MicroRNAs miR-146a/b negatively modulate the senescence-associated inflammatory mediators IL-6 and IL-8,” *Aging (Albany NY)* vol. 1, no. 4, pp. 402–11, 2009

15. M. Rottner, J. Freyssinet, and M. Martinez, “Mechanisms of the noxious inflammatory cycle in cystic fibrosis,” *Respiratory Research*, vol. 10, p. 23, 2009

16. S. S. Wang and R. Magnusson, “Theory and applications of guided-mode resonance filters,” *Appl. Opt.*, vol. 32, no. 14, pp. 2606–2613, 1993

17. S. Fan and J. D. Joannopoulos, “Analysis of guided resonances in photonic crystal slabs,” *Phys. Rev. B*, vol. 65, no. 23, 235112, 2002

18. Y. Ding and R. Magnusson, “Resonant leaky-mode spectral-band engineering and device applications,” *Opt. Express*, vol. 12, no. 23, pp. 5661–5671, 2004

19. M. Lu, S. S. Choi, U. Irfan, and B. T. Cunningham, “Plastic distributed feedback laser biosensor,” *Appl. Lett.*, vol. 93, no. 11, 111113, 2008

20. Y. Zhao, K. Liu, J. McClelland and M. Lu, “Enhanced photoacoustic detection using photonic crystal substrate,” *Appl. Phys. Lett.*, vol. 104, no. 16, 161110, 2014

APPENDIX A

PUBLICATIONS AND PRESENTATIONS

A.1 Peer Reviewed Journals

1. Y. Zhao, K. Liu, J. McClelland and M. Lu, "Enhanced photoacoustic detection using photonic crystal substrate," *Appl. Phys. Lett.*, vol. 104, no. 16, 161110, 2014

A.2 Conference Presentations

1. CLEO 2014, San Jose, California, June 9-13, 2014 (accepted for presentation)

APPLIED PHYSICS LETTERS **104**, 161110 (2014)

Enhanced photoacoustic detection using photonic crystal substrate

Yunfei Zhao,[1] Kaiyang Liu,[1] John McClelland,[2,3,4] and Meng Lu[1,3,a)]
[1]*Department of Electrical and Computer Engineering, Iowa State University, Ames, Iowa 50011, USA*
[2]*Ames Laboratory-USDOE, Ames, Iowa 50011, USA*
[3]*Department of Mechanical Engineering, Iowa State University, Ames, Iowa 50011, USA*
[4]*Department of Biochemistry, Biophysics, and Molecular Biology, Iowa State University, Ames, Iowa 50011, USA*

(Received 27 February 2014; accepted 9 April 2014; published online 23 April 2014)

This paper demonstrates the enhanced photoacoustic sensing of surface-bound light absorbing molecules and metal nanoparticles using a one-dimensional photonic crystal (PC) substrate. The PC structure functions as an optical resonator at the wavelength where the analyte absorption is strong. The optical resonance of the PC sensor provides an intensified evanescent field with respect to the excitation light source and results in enhanced optical absorption by surface-immobilized samples. For the analysis of a light absorbing dye deposited on the PC surface, the intensity of photoacoustic signal was enhanced by more than 10-fold in comparison to an un-patterned acrylic substrate. The technique was also applied to detect gold nanorods and exhibited more than 40 times stronger photoacoustic signals. The demonstrated approach represents a potential path towards single molecule absorption spectroscopy with greater performance and inexpensive instrumentation. © *2014 AIP Publishing LLC*. [http://dx.doi.org/10.1063/1.4872319]

Photoacoustic (PA) spectroscopy has attracted great interest since the mid-1970s due to its capability to non-invasively monitor light absorbing analytes over substantial ranges of concentrations.[1–4] Although laser-based PA detections exhibit a higher sensitivity as compared to optical absorption measured directly by transmission spectroscopy, it is always desirable to improve the signal-to-noise ratio to accurately quantify trace amounts of molecules. To maximize the signal-to-noise ratio of PA measurements, a variety of approaches have been studied for the purpose of amplifying acoustic output and suppressing noise. The reported signal enhancements arise from two major effects: acoustic resonance and optical resonance.[5–9] Notably, optical resonance-based methods utilize cavities, formed by high reflectivity mirrors or micro-/nanostructures, to increase optical path length and to result in enhanced absorption by the target molecule residing inside the cavity.[10]

To address the challenge of measuring solid substance at low concentrations or with low absorption coefficient, we propose to use a one-dimensional photonic crystal (PC) structure to increase light absorption and to generate a stronger PA output consequently. The PC substrate, comprised of a periodically nanostructured dielectric thin film, supports guided-mode resonance (GMR), also known as a leaky mode.[11–13] The GMR effect occurs when the PC substrate is illuminated under resonance conditions and leads to intensified local field with respect to the electric field strength of the incident light. By spectrally overlapping a GMR resonance wavelength with the absorption band of the analyte, one can obtain an increase in the optical absorption. Previous publications have demonstrated the application of a PC substrate for fluorescence-based detections.[14–17] Several compelling features of the PC are of practical importance for the development of an enhanced detection scheme to be used in PA analysis. The PC structure can be tailored to tune the GMR wavelength from visible to mid-infrared, and thus the GMR wavelength can align with the absorption bands of a wide variety of substances.[18–20] It is inexpensive to fabricate large surface areas of PC substrates using optically transparent materials and to incorporate them into a PA detection instrument. In addition, the PC substrate is made using polymer material with low thermal conductivity that prevents heat dissipation and ensures strong PA signal output. This Letter reports design and experimental characterization of a PC sensor for enhanced PA detection of organic dye molecules and metal nanoparticles (NPs).

A cross-sectional diagram (not to scale) of the PC structure adopted for the PA experiment is shown in Fig. 1(a). The 1D PC, comprised of a linear grating surface structure, was fabricated using a nanoreplica molding process approach that has been described in detail previously.[21] Briefly, a silicon mold bearing a grating pattern was fabricated by electron-beam lithography and reactive ion etching, with surface area of $2\,\text{mm} \times 2\,\text{mm}$. Liquid ultra-violet curable epoxy (UVCP, NOA 85, Norland Product Inc.) was squeezed between the silicon mold and a transparent acrylic film and was solidified by exposing to UV light through the plastic substrate. Once separated from the silicon mold, the substrate film with the cured epoxy (refractive index, $n_{UVCP} = 1.46$) carried a grating pattern with a period of $\Lambda = 400\,\text{nm}$, duty cycle of 60%, and a depth of $d = 60\,\text{nm}$. The grating surface was coated with a 100 nm titanium dioxide (TiO_2) dielectric film using an electron beam evaporator. The TiO_2 thin film (refractive index, $n_{TiO2} = 2.0$) provided light confinement for the GMRs. The design parameters were chosen to maximize the strength of optical resonance at the excitation wavelength and to provide strong local field intensity at the PC surface.

A schematic of the detection instrument is shown in Figure 1(b). The setup consists of a HeNe laser source with emission at $\lambda = 632.8\,\text{nm}$, an optical chopper, a tunable mirror

a)Electronic address: menglu@iastate.edu

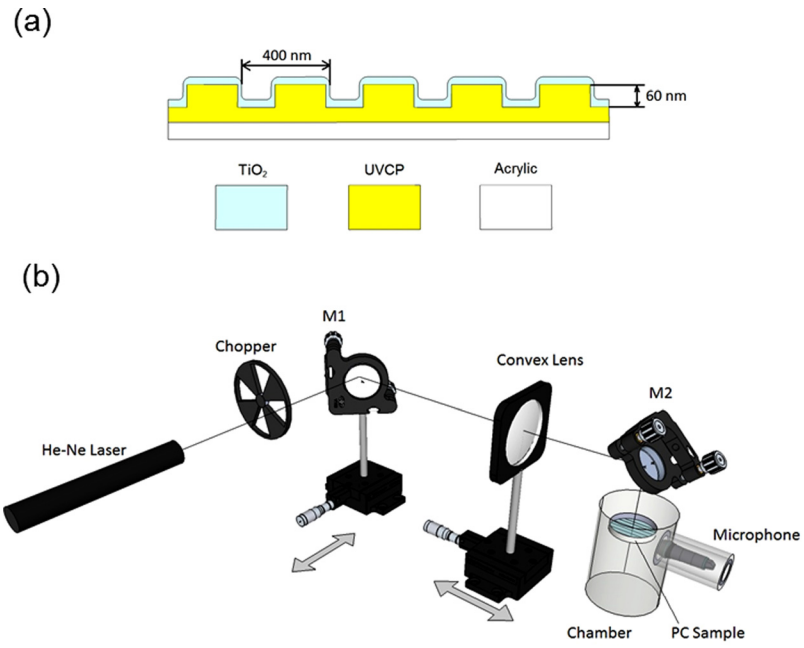

FIG. 1. (a) Schematic cross section of the PC structure (not to scale). The grating structure is fabricated using replica-molding process with period and duty cycle of 400 nm and 60%, respectively. (b) Complete optical layout of the experimental set-up. Linear polarized laser excitation at 632.8 nm was intensity modulated by a mechanical chopper wheel and reflected by a mirror (M1) that is translated horizontally to adjust the angle of incidence. A long-focus lens was used to focus the laser beam onto the PC sensor located on the topside of the PA chamber. The diameter of the focused laser spot was around 80 μm.

(M1) mounted on a translation stage, a convex lens, a second mirror (M2), and a PA analysis module (PAC 200 MTEC Photoacoustic Inc.) that incorporates the PC substrate. During the test, the output power of the HeNe laser was kept at 5 mW. The chopper modulated the laser emission with a square wave pattern at a frequency of 13 Hz. To excite a GMR at the desired wavelength (632.8 nm), the excitation light should illuminate the PC substrate at a specific angle of incidence. In the system, the mirror (M1) and the convex lens were utilized to tune the incident angle, defined in the direction perpendicular to the orientation of the grating. The convex lens with a focal length of 150 mm was fixed at a position so that its focal point was exactly on the sample. Translation of the M1 enabled adjustment of the incident angle from $-7.2°$ to $7.2°$. As the excitation light was efficiently coupled into the GMR, the intensified near field on the PC surface occurred and consequently generated a stronger photothermal effect.

The PA detection experiments require a sealed chamber to eliminate the ambient vibration noise. To combine the PC and the chamber, we attached the PC sensor onto an acrylic window that sealed the chamber with the PC facing the inside of the chamber. An acoustic transducer, a microphone (4176, Brüel & Kjær A/s), was connected to the chamber to measure photoacoustic pressure oscillations. During the experiments, light absorbing materials coated on the PCs absorbed light energy and generated pressure oscillations in the atmosphere of the chamber due to absorption induced heating. These pressure oscillations were converted to a voltage output by the microphone and were subsequently quantified using an oscilloscope (TDS2000, Tektronix). In the experiment, PA outputs were calculated by averaging voltage amplitudes in the waveforms obtained from the oscilloscope.

In order to characterize the enhancement performance of the fabricated PC, a PA detection experiment using a light absorbing dye was carried out on the PC substrate. The PC substrate was cleaned with isopropyl alcohol, de-ionized (DI) water, and dry N_2, and the organic dye (Epolight 5262, Epolin Inc.) was dissolved in methanol and made up to concentrations in the range from 50 μg/ml down to 1 μg/ml. The dye solutions were drop-cast on the substrates and dried before use. To identify the resonant angle, we measured the laser transmission efficiency through the PC as a function of incident angle (θ_i) as shown in Figure 2, where the dip in the transmission curve corresponds to the resonant angle (θ_r), in this case $\theta_r = 3.5°$. Plotted as the red curve in the same figure is the PA signal from 5 μg/ml dye absorbed on the PC surface. Figure 2 clearly illustrates how the optical resonance (low transmission efficiency) results in a stronger PA output. After the subtraction of background signal, the PA signal at $\theta_r = 3.5°$ is 5.8 V that is more than 10× higher than the PA signal measured away from this angle. Furthermore, Figure 3 shows the PA signals measured using a 2-fold dilution series of a total of six dye concentrations in the aforementioned range of concentration. In Figure 3, the red curve represents PA signals measured under resonance condition, when the GMR was excited at the angle of incidence of $\theta_r = 3.5°$. As a reference, the black curve in Figure 3 shows the PA signal

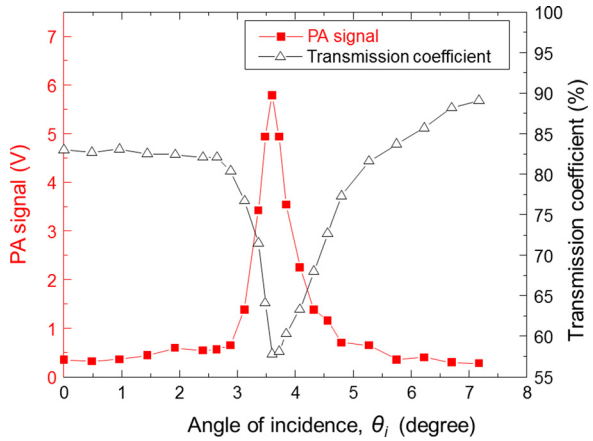

FIG. 2. A comparison of the PA signal (red square) to the normalized transmission coefficient (black triangle) measured as a function of incident angle tuned from 0° to 7.2°. The normalized transmission coefficient of PC substrate was measured using a TM-polarized HeNe laser source.

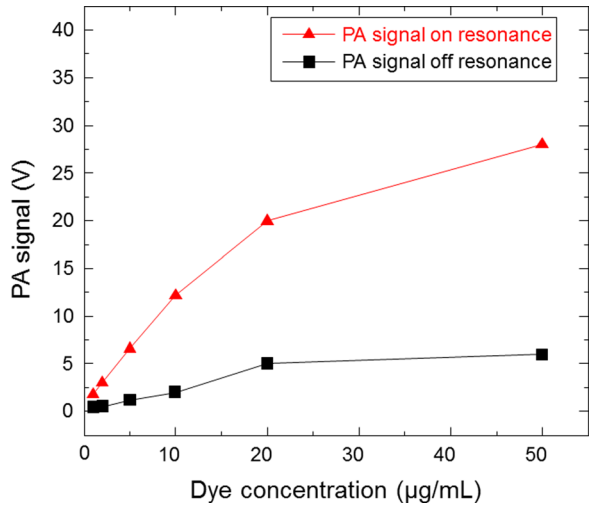

FIG. 3. PA signal intensity for a dilution series of absorbing dyes deposited on a PC substrate. The PC substrate was illuminated at 3.5° as the on resonance case (red triangle) and at 7° as the off resonance case (black square).

outputs of the dyes when the HeNe laser illuminated the PC under "off-resonance" condition ($\theta_i = 7°$). At the dye concentrations below 20 μg/ml, both curves vary linearly in terms of dye concentration. In this linear range, the sensitivity is 1.25 V/(μg/ml) when the PC is on resonance as compared to 0.18 V/(μg/ml), when it is off resonance, resulting in an averaged enhancement of 7-fold. Figure 3 clearly demonstrates that the PC enhancement provided easily distinguishable PA outputs and an extended range of quantification for the dyes at low concentrations. At higher concentrations, the PA signal started to saturate and the enhancement factor was reduced to 5.3 because the loss induced by the absorption of dye molecules quenched the PC resonance and reduced the PC enhancement factor.

Having demonstrated the PA signal enhancement of PC substrate to organic light absorbing molecules, we next exploited the PC resonance for the PA detection of metal NPs immobilized on the PC surface. Due to the localized surface plasmon resonance, the metal NPs exhibited tunable absorption in visible and near IR wavelength range.[22] Finite difference time domain (FDTD) simulation was utilized to calculate the near field distributions upon the PC sensor, which was coated with metal nanoparticles. The cross-sectional views of electric field intensity for a gold nanoparticle (AuNP) on a flat acrylic substrate, a blank PC sensor, and an AuNP on PC sensor are shown in Figure 4(a). The dimensions of the simulated PC structure are specified in Figure 1(a) and the gold nanoparticle has an axial diameter of 25 nm and length of 60 nm. In the FDTD simulation, the incident field was set as a plane wave propagating towards the PC surface at the resonant wavelength of $\lambda_r = 632$ nm and the coupling angle of $\theta_r = 0°$. The periodic boundary conditions were used in the grating plane to define the computational region. The scale bars on the right side represent resonant electric field intensity ($|\mathbf{E}|^2$) levels normalized with respect to the incident electric field intensity. As shown in Figure 4(a), the evanescent field within a hundred-nanometer range above the PC surface is significantly enhanced. The resonant field of the PC sensor is not significantly disturbed by the presence of the AuNP and the field intensity near the AuNP is further intensified due to the plasmonic resonance. Figure 4(b) compares the calculated absorption spectrum of AuNPs on PC and acrylic substrates. At the resonant wavelength, the

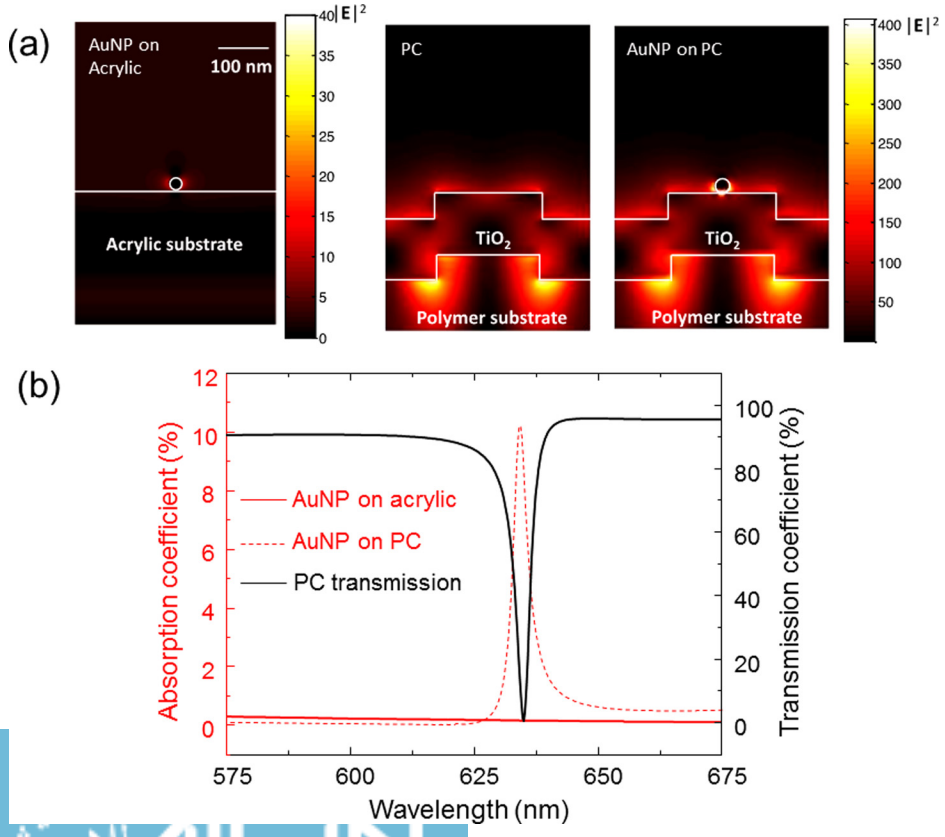

FIG. 4. (a) Spatial distribution of the simulated near-field intensity within a single period of the PC grating, for an AuNP on a flat acrylic substrate, a blank PC substrate, and an AuNP on a PC surface, respectively. The upper horizontal white lines indicate the substrate surfaces and the white circles represent the surface of the AuNP. (b) Calculated absorption spectra of AuNPs on acrylic and PC substrates. The modeled transmission spectrum shows the correlation between the GMR mode and the enhanced optical absorption of AuNPs on the PC sensor. The surface density of the AuNPs is 6.25 NPs/μm^2.

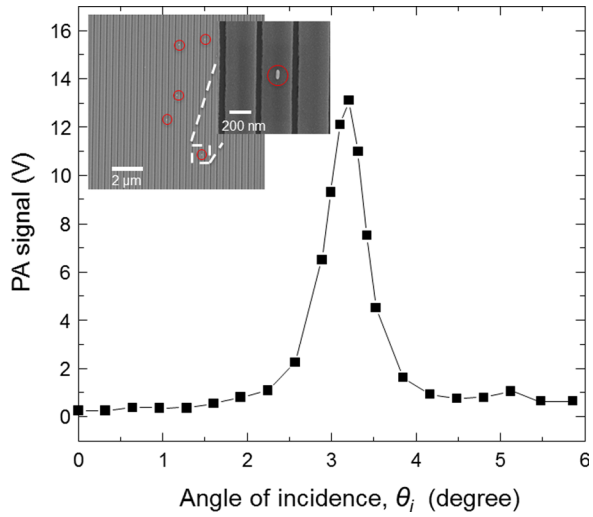

FIG. 5. Measured PA signal intensity of AuNPs on a PC surface as a function of incident angle between 0° and 6°. Inset: SEM image of the PC substrate with Au nanorods dispersed at 10^{10} NPs/ml.

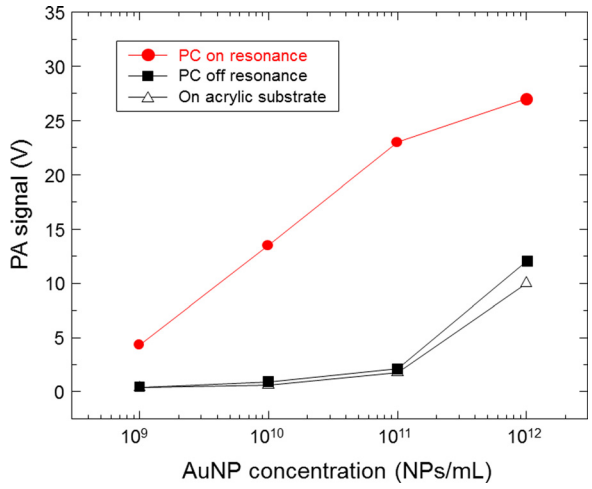

FIG. 6. PA signal intensity for a dilution series of gold nanoparticles deposited on a PC substrate and an acrylic substrate, respectively. The PC substrate was illuminated at 3.2° for on-resonance (red circle) and at 7° for off-resonance (black square).

absorption of AuNPs on the PC substrate becomes 60× stronger than the same AuNPs on the planar acrylic substrate.

Detection of metal NPs was characterized by depositing gold nanorods onto the PC surface. Gold nanoparticle samples were prepared by suspending gold nanorods of approximately 25 nm axial diameter (A12-25-650, Nanopartz Inc.) in DI water. To deposit the AuNPs, 10 μl spots of these samples were pipetted onto PC substrates and allowed to dry in air before measuring. A scanning electron microscopy image of PC coated with AuNPs at the concentration of 10^{10} NPs/ml is shown in the inset of Figure 5 where only a few nanorods are present within a 10 μm × 10 μm area. Figure 5 illustrates the intensity of PA signal measured as a function of the incident angle of the excitation laser. The laser was scanned from $\theta_i = 0°$ to 7.2° and coupled into the GMR at $\theta_i = 3.2°$. Measured under resonant conditions, the intensity of PA signal is over 13 V that is 40× stronger than the PA output (0.33 V) measured without utilizing the PC resonance.

The PC provides substantial increase in the PA output of AuNPs and also significant reduction in the PA detection limit. In order to demonstrate this, samples coated with AuNPs at a range of concentrations (10^{12} NPs/ml, 10^{11} NPs/ml, 10^{10} NPs/ml, and 10^{9} NPs/ml) are measured for the PC illuminated on-resonance ($\theta_i = 3.2°$), off-resonance ($\theta_i = 7°$), and for the control acrylic slides. The measured PA signals with background subtracted are compared in Figure 6. The lowest detectable concentration on the acrylic substrate (10^{10} NPs/ml) is reduced by one order of magnitude to 10^{9} NPs/ml on PC substrate. At higher concentrations, the amplification factor becomes weaker due to the quench of optical resonance caused by the absorption of AuNPs. The PC sensor offers the capability to detect less than 10 nanorods within a 100 μm^2 surface area.

In summary, a 1D PC substrate has been characterized for its capability to enhance the PA signal from light absorbers deposited onto the sensor surface. The PC sensor was incorporated into a PA measurement chamber and illuminated by a HeNe laser with the angle of incidence tuned to excite the GMR. The strengthened local field associated with the resonant mode increased the optical absorption of analytes deposited on the PC and resulted in an enhanced PA signal by factors of 10× and 40× for the organic light absorber and the gold nanorods, respectively. The enhanced PA signal consequently reduced the detection limit of metal nanoparticles by one order of magnitude. The PC substrate demonstrated here represents a powerful and practical approach for highly sensitive PA detection and would be improved further for sensors produced over substantially large surface area with higher quality factors. In the future work, this technique will be exploited to facilitate the quantification of metal nanoparticles functionalized with recognition molecules, enabling a promising approach for diagnostic test and environmental monitoring.[23]

This research was supported by the start-up funding from the Iowa State University. The authors would like to acknowledge Dr. Wai Y. Leung of Microelectronics Research Center at Iowa State University for the technical supports.

[1]A. Rosencwaig, *Photoacoustics and Photoacoustic Spectroscopy* (Wiley, New York, 1980).
[2]J. F. McClelland, Anal. Chem. **55**(1), 89A–105A (1983).
[3]A. C. Tam, Rev. Mod. Phys. **58**(2), 381–431 (1986).
[4]H. Zhang, K. Maslov, G. Stoica, and L. Wang, Nat. Biotechnol. **24**(7), 848–851 (2006).
[5]A. Miklos, P. Hess, and Z. Bozoki, Rev. Sci. Instrum. **72**, 1937–1955 (2001).
[6]V. Koskinen, J. Fonsen, K. Roth, and J. Kauppinen, Vib. Spectrosc. **48**(1), 16–21 (2008).
[7]M. Hippler, C. Mohr, K. A. Keen, and E. D. McNaghten, J. Chem. Phys. **133**(4), 044308 (2010).
[8]A. Kachanov, S. Koulikov, and F. K. Tittel, Appl. Phys. B **110**, 47–56 (2013).
[9]A. A. Kosterev, Yu. A. Bakhirkin, R. F. Curl, and F. K. Tittel, Opt. Lett. **27**(21), 1902–1904 (2002).
[10]H. Lin, Y. Zou, and J. Hu, Opt. Lett. **37**(8), 1304–1306 (2012).
[11]S. S. Wang and R. Magnusson, Appl. Opt. **32**(14), 2606–2613 (1993).
[12]S. Fan and J. D. Joannopoulos, Phys. Rev. B **65**(23), 235112 (2002).
[13]Y. Ding and R. Magnusson, Opt. Express **12**(23), 5661–5671 (2004).
[14]D. Neuschaefer, W. Budach, C. Wanke, and S. D. Chibout, Biosens. Bioelectron. **18**, 489–497 (2003).
[15]V. Chaudhery, S. George, M. Lu, A. Pokhriyal, and B. T. Cunningham, Sensors Journal **13**, 5561–5584 (2013).

[16]C.-S. Huang, S. George, M. Lu, V. Chaudhery, R. Tan, R. C. Zangar, and B. T. Cunningham, Anal. Chem. **83**(4), 1425–1430 (2011).
[17]J. H. Lin, C. Y. Tseng, H. C. Kan, and C. C. Hsu, Opt. Express **21**(20), 24318–24325 (2013).
[18]A. Pokhriyal, M. Lu, C.-S. Huang, S. C. Schulz, and B. T. Cunningham, Appl. Lett. **92**(12), 121108 (2010).
[19]A. Pokhriyal, M. Lu, V. Chaudhery, C.-S. Huang, S. Schulz, and B. T. Cunningham, Opt. Express **18**(24), 24793–24808 (2010).
[20]J.-N. Liu, M. V. Schulmerich, R. Bhargava, and B. T. Cunningham, Opt. Express **19**(24), 24182–24197 (2011).
[21]M. Lu, S. S. Choi, U. Irfan, and B. T. Cunningham, Appl. Lett. **93**(11), 111113 (2008).
[22]J. N. Anker, W. P. Hall, O. Lyandres, N. C. Shah, J. Zhang, and R. P. Van Duyne, Nature Mater. **7**, 442–453 (2008).
[23]K. A. Willets and R. P. Van Duyne, Annu. Rev. Phys. Chem. **58**, 267–297 (2007).